NRL Report 7779

Comparison of a Cube-Textured-Nickel and a Nickel-200 Magnetostrictive Ring Transducer

JOEL A. SINSKY

Transducer Branch
Acoustics Division

August 12, 1974

NAVAL RESEARCH LABORATORY
Washington, D.C.

REPORT DOCUMENTATION PAGE

READ INSTRUCTIONS BEFORE COMPLETING FORM

1. REPORT NUMBER: NRL Report 7779	2. GOVT ACCESSION NO.
3. RECIPIENT'S CATALOG NUMBER	
4. TITLE *(and Subtitle)*: COMPARISON OF A CUBE-TEXTURED-NICKEL AND A NICKEL-200 MAGNETOSTRICTIVE RING TRANSDUCER	5. TYPE OF REPORT & PERIOD COVERED: Interim report on a continuing NRL Problem
	6. PERFORMING ORG. REPORT NUMBER
7. AUTHOR(s): Joel A. Sinsky	8. CONTRACT OR GRANT NUMBER(s): NRL Problem S02-19
9. PERFORMING ORGANIZATION NAME AND ADDRESS: Naval Research Laboratory, Washington, D.C. 20375	10. PROGRAM ELEMENT, PROJECT, TASK AREA & WORK UNIT NUMBERS: XF 11-121-100, Task 1-01-01
11. CONTROLLING OFFICE NAME AND ADDRESS: Department of the Navy, Naval Electronics Systems Command, Code 320, Washington, D.C. 20360	12. REPORT DATE: August 12, 1974
	13. NUMBER OF PAGES: 32
14. MONITORING AGENCY NAME & ADDRESS*(if different from Controlling Office)*	15. SECURITY CLASS. *(of this report)*: UNCLASSIFIED
	15a. DECLASSIFICATION/DOWNGRADING SCHEDULE

16. DISTRIBUTION STATEMENT *(of this Report)*

Approved for public release; distribution unlimited.

17. DISTRIBUTION STATEMENT *(of the abstract entered in Block 20, if different from Report)*

18. SUPPLEMENTARY NOTES

19. KEY WORDS *(Continue on reverse side if necessary and identify by block number)*

Magnetostrictive materials
Magnetostriction transducers
Free-flooded ring
Underwater sound sources
Acoustic measurements

20. ABSTRACT *(Continue on reverse side if necessary and identify by block number)*

The magnetic and magnetostrictive properties of a magnetostrictive scroll-wound ring transducer made from cube-textured nickel were measured and compared to the corresponding properties of a ring transducer made from conventional Nickel 200. Both transducers were separately excited in air at low-power linear drive levels with varying induction fields of magnetization, and their electrical input impedances were measured. Some in-water measurements were also made on the two rings at nearly optimum values of induction field. The data obtained can be used to choose the type of ring and the induction-field level of operation which will best satisfy a given requirement.

CONTENTS

COMPARISON OF A CUBE-TEXTURED-NICKEL AND A NICKEL-200 MAGNETOSTRICTIVE RING TRANSDUCER

INTRODUCTION

The magnetic and magnetostrictive properties of a magnetostrictive scroll-wound ring transducer made from cube-textured nickel developed by the International Nickel Company (INCO) were measured and compared to the corresponding properties of a conventional-nickel ring transducer. The conventional-nickel ring was fabricated at the Naval Underwater Systems Center, New London, Connecticut, and the cube-textured ring of nearly identical dimensions was fabricated at INCO. Both transducers were separately excited in air under identical physical conditions but with varying induction fields, and their electrical input impedances were measured on a (Scientific Atlanta) Pulse Vector Immittance Meter. Elastic and magnetostrictive properties of the rings were derived from the impedance measurements and plotted as a function of induction field to show their induction-field dependence and to facilitate comparison of the rings' properties. Some in-water measurements were also made on the two rings at nearly optimum values of induction field. The data obtained can be used to choose the type of ring and the induction-field level of operation which will best satisfy a given requirement.

APPARATUS

The ring transducers used were wire-wound magnetostrictive cores (Fig. 1). The core materials were conventional Nickel 200 which is also called *A* Nickel and the INCO cube-textured nickel (CTN). The ring cores were scroll wound, which means that they were made by winding a metal strip about a mandrel and using a bonding agent to hold them permanently. The Nickel-200 strip was 0.007 inch thick and the INCO CTN strip was 0.008 inch thick. Table 1 gives the average dimensions of the finished cores. The accuracy of the measurements was ±0.0001 m and ±0.0001 kg.

Each of the cores was separately mounted as shown in Fig. 1. The mounting structure was designed to hold a core in a fixed position in the windings while providing the least possible clamping of the core and to be acoustically invisible in the excitation frequency range of interest. The 144 toroidal turns of No. 18 Teflon-insulated wire were supported by four copper hoops above and below the ring core, and the hoops in turn were supported by two sets of three spokes emanating from hubs at the center of the ring transducer. The hubs were held apart and the entire structure was kept rigid by a threaded 1/4-inch bolt and four nuts. The motion of the core was isolated from the supporting structure by pads of rho-c rubber. The toroidal windings were kept uniformly spaced around the ring by 0-ring stock which was weaved circumferentially through the windings. The average cross-sectional area enclosed in the windings was

Note: Manuscript submitted June 3, 1974.

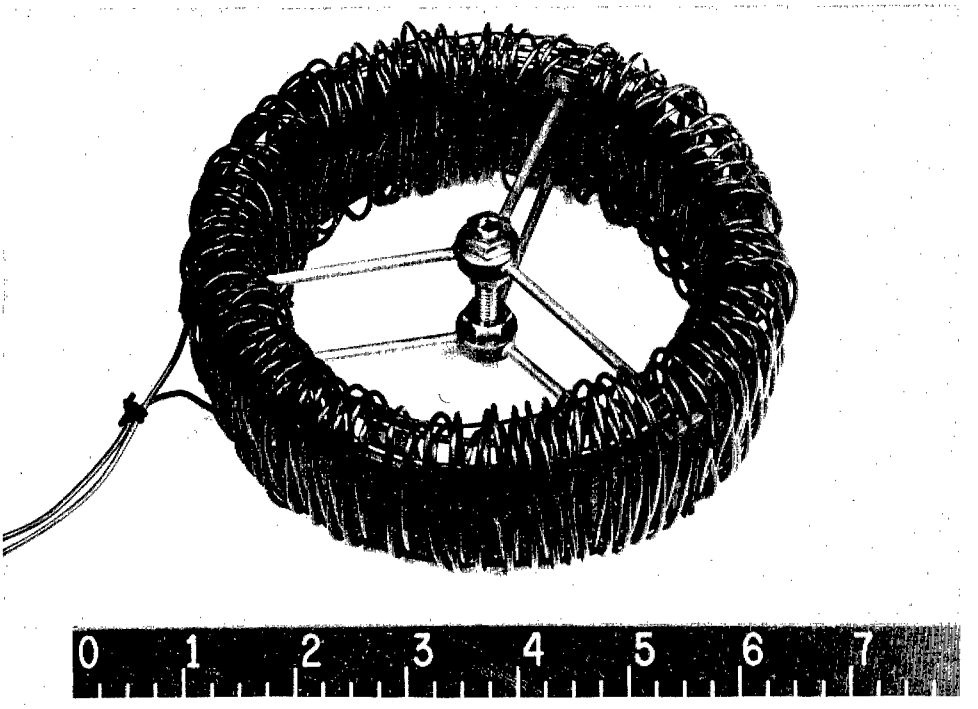

Fig. 1 — A transducer

Table 1
Average Dimensions and Masses of the Finished Cores

Ring	Outside Diameter (m)	Inside Diameter (m)	Height (m)	Mean Radius (m)	Mass (kg)
CTN	0.1382	0.1249	0.02029	0.06578	0.4591
Nickel 200	0.1378	0.1250	0.01942	0.06573	0.4338

$A_{coil} = 1.219 \times 10^{-3}\ m^2$ for the CTN ring,

$A_{coil} = 1.070 \times 10^{-3}\ m^2$ for the Nickel-200 ring.

For the air and water measurements the rings were hung with the center bolt vertical by single pieces of stiff single-conductor wire attached to the center bolt.

Each ring was simultaneously excited by a dc magnetizing current and an ac driving current. The blocking circuit which isolated the ac current source from the dc current source is diagrammed in Fig. 2.

The circuit block diagram of the transducer driving system is shown in Fig. 3. The in-air impedance measurements were done CW; therefore the pulse timing generator and the

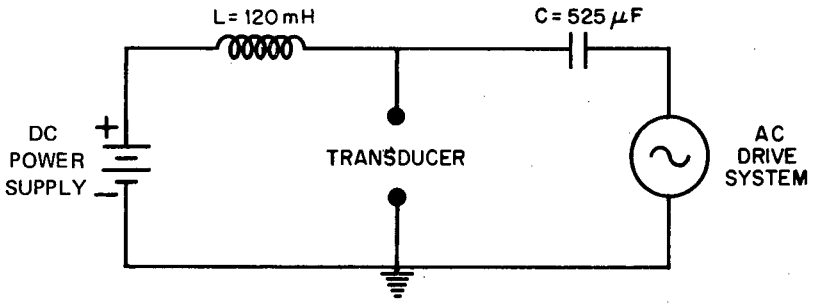

Fig. 2 — Blocking circuit to isolate the current sources

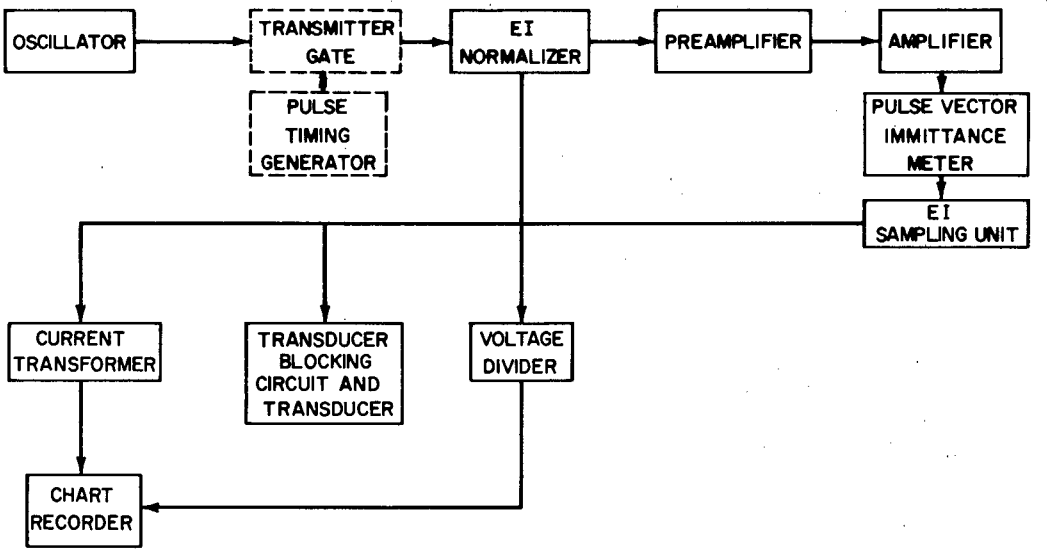

Fig. 3 — Transducer driving system

transmitter gate in the driving system were switched off. They were switched on for the in-water measurements, when the pulse-modulated driving signal and the Pulse Vector Immittance Meter allowed determination of free-field steady-state impedances in the confined space of the NRL Acoustic Research Tank.

The Pulse Vector Immittance Meter measured the input electrical resistance and reactance of the transducer and blocking circuit under conditions of CW or pulsed current excitation. The dc magnetizing current was varied during the experiment to provide varying induction-field levels in the ring cores. The level of the ac drive current however was held constant at 15 milliamperes rms for the entire experiment by a current normalizer. Two fans were directed at the transducers during the in-air measurements to circulate air through the toroidal windings and around the ring core and thereby reduce the heating of the windings and core, particularly for operation at high induction-field levels. Nevertheless the ring cores became significantly warmer when the magnetizing current exceeded 10 amperes. The Pulsed Vector Immittance Meter was calibrated each day of the experiment with a standard 500-microhenry choke at 10 kHz. The rings were demagnetized between changes of the level of the dc magnetizing current for the measurements at low induction-field levels.

EXPERIMENTAL DATA

An experimental run on a ring transducer corresponded to input electrical impedance measurements at various frequencies of ac excitation for a single value of dc magnetizing current. Ten runs were made on each of the two rings in air, and the values of magnetizing currents were chosen so as to apply roughly the same range of induction fields in the rings. Table 2 gives the applied dc magnetizing current and the corresponding calculated magnetic-field intensity and induction-field intensity by using B-H curves for the ring cores. The values given are in units of measurement most familiar to transducer engineers: amperes, oersteds (1 Oe $\approx$ 80 A/m), and kilogauss (1 kG $\equiv$ 0.1 tesla). The induction-field levels for each ring are approximately in the range 1 to 5 kG, and they are spaced evenly throughout the range. A direct comparison of the variation of the magnetostrictive parameters of the rings versus induction field is thereby facilitated.

Table 2
Current, Magnetic-Field Intensity, and Induction-Field Level for Each Run

Run	CTN Ring			Nickel-200 Ring		
	I (A)	H_3 (Oe)	B_3 (kG)	I (A)	H_3 (Oe)	B_3 (kG)
1	0.73	3.2	1.0	0.30	1.3	0.92
2	0.91	4.0	1.5	0.45	2.0	1.3
3	1.1	4.8	2.0	0.65	2.9	1.7
4	1.4	6.1	2.5	1.0	4.4	2.2
5	2.0	8.8	3.1	1.6	7.0	2.8
6	4.0	18	3.8	2.9	13	3.6
7	6.0	26	4.2	3.8	17	3.9
8	8.0	35	4.4	4.4	19	4.1
9	12	53	4.6	5.5	24	4.4
10	20	88	5.0	7.8	34	4.8

For each run the impedance was measured at seven frequencies (1, 2, 3, 4, 5, 6 and 7 kHz), well below the radial resonance frequency of the rings. Approximately 30 values of impedance were then measured at or near radial resonance to define the impedance circle resulting from a plot of electrical input reactance versus electrical input resistance. Finally some values of impedance were measured at frequencies well above the radial resonance frequency of the rings. During each run a plot of input reactance versus input resistance was drawn by a chart recorder as the numerical values of these quantities were being recorded from the Pulse Vector Immittance Meter. The simultaneous plot, though not used for data, was useful in visually indicating the frequencies at which impedance should be recorded. The data were corrected for the contribution to the total input electrical impedance from the blocking circuit.

The resulting corrected numerical data for a typical run on the CTN ring—dc magnetizing current = 4.0 amperes (induction-field level = 3.8 kilogauss) and ac driving current = 15 milliamps—are given in Table 3a. The resulting corrected numerical data for

a typical run on the Nickel-200 ring—dc magnetizing current = 3.8 amperes (induction-field level = 3.9 kilogauss) and ac driving current = 15 milliamps—are given in Table 3b. Figure 4a shows the impedance circle of the CTN ring, and Fig. 4b shows the impedance circle of the Nickel-200 ring; these are plots of the data for frequencies near resonance in Tables 3a and 3b respectively. Each point on the plots corresponds to a specific frequency of ring excitation, and the total electrical input impedance at the frequency is the length of a vector drawn from the origin of coordinates to the point. Similar data were recorded for each of the 10 runs on the CTN ring and each of the 10 runs on the Nickel-200 ring.

In addition to the 20 in-air runs described, one run on each ring was done in water. The water run on the CTN ring was at 4.0 amperes dc magnetizing current and 15 milliamperes ac pulsed drive, and the water run on the Nickel-200 ring was 3.8 amperes dc magnetizing current and 15 milliamperes ac pulsed drive. The purpose of the in-water runs was to verify a mathematical model of a free-flooded magnetostrictive ring transducer (NRLEIGSHIP) which predicts the in-water behavior of a ring from empirical data derived from the ring's in-air behavior. The in-water runs also provide a comparison of the rings' performance in water under approximately equal dc induction levels and equal ac levels of drive. Table 4a gives the electrical input resistance and reactance versus frequency of the CTN ring near water radial resonance for 4.0 amperes dc magnetizing current, and Table 4b gives analogous data for the Nickel-200 ring at 3.8 amperes dc magnetizing current. Figures 5a and 5b show the electrical input reactance versus resistance curves plotted from the data.

ANALYSIS

An approximate expression for the total electrical input impedance Z_T of a magnetostrictive ring transducer in air is derived as a function of the electrical and magnetostrictive properties and the dimensions of the ring from Butterworth and Smith's equivalent circuit of a magnetostrictive oscillator [1]:

$$Z_T = r_w + \frac{jfN^2 4\pi \times 10^{-7}}{a(A_{\text{coil}} - A_0)^{-1}} + \frac{jfN^2 \mu_{33}^s A_0 \chi}{a} + \left[\frac{\mu_{33}^s N g_{33} A_0 \chi}{a S_{33}^B}\right]^2 \left[\frac{1}{R_m + jX_m}\right], \quad (1)$$

where

$$R_m = R_{mp} + \frac{A_0 k_{33}^2 \chi_I}{a f S_{33}^B}$$

and

$$X_m = 2\pi f M - \frac{A_0(1 - k_{33}^2)}{a f S_{33}^B}.$$

This expression for Z_T is written in a form compatible with all of the variables in the MKS units of measurement (also compatible with the Système International d'Unités, or SI units). The term r_w, the dc resistance of the toroidal windings, is typically less than 1 ohm and can be neglected. The second term on the right, which Butterworth and Smith

Table 3a
Impedances of the CTN Ring During Run 6 (Table 2): I_{dc} = 4.0 A

Frequency (Hz)	Resistance (Ω)	Reactance (Ω)
Frequencies Below Resonance		
1000	0.8	1.4
2000	0.8	2.8
3000	0.8	4.4
4000	0.8	5.9
5000	0.9	7.6
6000	1.0	9.1
7000	1.1	10.9
Frequencies Near Air Resonance		
8000	1.0	13.5
8500	1.6	16.3
9000	6.0	28.6
9119	28.5	46.8
9122	29.8	47.3
9125	31.4	47.7
9128	34.3	48.2
9131	36.4	48.4
9134	39.0	48.5
9137	42.0	48.4
9140	45.0	48.1
9144	49.7	47.1
9150	58.8	43.5
9162	73.0	29.7
9165	75.8	24.1
9168	76.9	21.3
9171	78.7	14.1
9174	79.2	9.0
9177	78.9	2.3
9180	77.8	-2.7
9184	76.0	-7.9
9206	52.7	-30.2
9209	49.2	-31.2
9212	46.0	-31.9
9215	42.6	-32.4
9218	41.0	-32.5
9221	37.5	-32.5
9224	35.3	-32.4
9227	33.3	-32.2
9230	30.8	-31.7
9233	27.8	-30.9
9239	24.2	-29.7
9246	20.9	-28.1
9321	5.1	-11.4
9500	0.9	1.9
10000	0.6	9.4
11000	0.8	13.1

Table 3b
Impedances of the Nickel-200 Ring During Run 7 (Table 2): I_{dc} = 3.8 A

Frequency (Hz)	Resistance (Ω)	Reactance (Ω)
Frequencies Below Resonsnce		
1000	0.9	2.3
2000	0.8	4.5
3000	0.9	7.0
4000	1.0	9.3
5000	1.2	11.8
6000	1.4	14.1
7000	1.8	16.7
Frequencies Near Air Resonance		
8000	2.0	18.7
9000	2.5	21.8
10000	3.5	26.0
11000	8.7	38.4
11333	36.3	62.4
11345	40.0	63.2
11360	46.2	64.2
11364	49.1	64.7
11368	50.3	64.6
11371	51.5	64.8
11374	52.5	65.8
11377	54.5	65.5
11381	56.4	65.4
11384	58.7	65.2
11388	60.7	64.7
11392	63.2	64.2
11396	65.7	63.7
11401	69.6	62.7
11455	110.9	26.5
11459	112.6	21.8
11462	113.1	16.9
11466	114.2	12.8
11469	114.6	8.7
11472	114.0	3.9
11475	114.0	0.4
11478	113.2	-2.9
11481	112.4	-6.8
11485	111.2	-12.0
11525	78.5	-47.0
11532	71.1	-49.2
11535	66.7	-50.0
11538	64.3	-50.4
11541	61.0	-50.6
11544	58.6	-50.8
11547	55.8	-50.8
11550	53.7	-50.6
11554	51.5	-50.4
11558	47.2	-49.7
11561	44.8	-49.1

Table 3a—Continued

Frequency (Hz)	Resistance (Ω)	Reactance (Ω)
Frequencies Above Resonance		
12000	1.4	15.2
13000	1.7	16.8
14000	1.7	18.3
15000	1.8	19.7
16000	1.9	21.0
17000	2.1	22.2
18000	2.1	23.5
19000	1.9	24.8
20000	1.6	26.1

Table 3b—Continued

Frequency (Hz)	Resistance (Ω)	Reactance (Ω)
Frequencies Above Resonance		
13000	2.2	21.7
14000	2.9	26.1
15000	3.5	29.0
16000	4.0	31.6
17000	4.5	33.9
18000	4.8	36.3
19000	5.0	38.6
20000	4.9	41.0

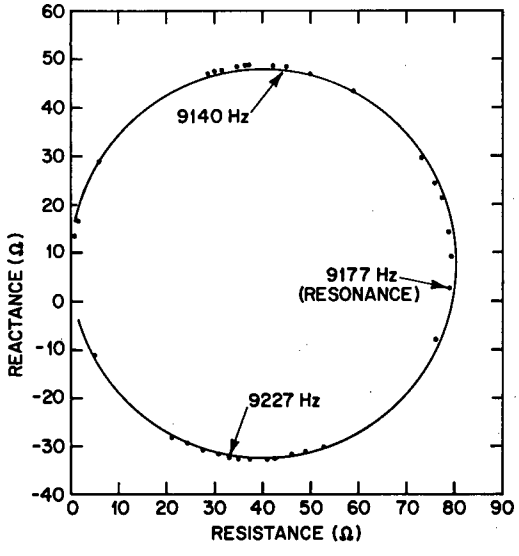

Fig. 4a — Electrical input impedance of the CTN Ring near air resonance with I_{dc} = 4.0 A (plotted from Table 3a)

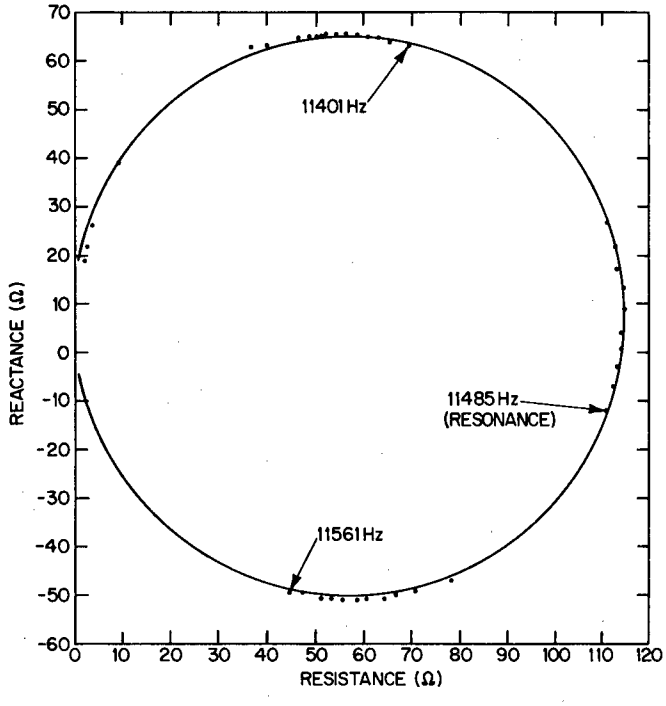

Fig. 4b — Electrical input impedance of the Nickel-200 ring near air resonance with I_{dc} = 3.8 A (plotted from Table 3b)

neglect, represents the leakage magnetic flux and is negligible if the cross-sectional area of the windings A_{coil} is not much greater than the cross sectional area of the core A_0 and if the reversible permeability of the core is large compared to that of air and water. In this experiment the leakage-flux term must be included because it is not negligible with respect to the total impedance off resonance for the high-induction-field runs. The first three terms on the right in Eq. (1) are independent of the magnetostrictive and motional properties of the ring. They represent the core impedance that would be obtained if the ring could be rigidly clamped. The fourth term on the right is the motional impedance term. In this equation f is the frequency of oscillation, N is the number of turns of wire

Table 4a
Impedances of the CTN Ring Near Radial Resonance for the Run in Water: I_{dc} = 4.0 A

Frequency (Hz)	Resistance (Ω)	Reactance (Ω)	Frequency (Hz)	Resistance (Ω)	Reactance (Ω)
6000	1.0	9.4	7782	7.1	8.1
7000	2.0	12.3	7792	7.0	8.0
7100	2.6	12.8	7800	7.0	8.0
7200	3.1	13.2	7810	6.8	7.8
7300	4.2	13.7	7822	6.7	7.7
7330	4.5	13.7	7833	6.6	7.7
7360	5.0	13.8	7843	6.4	7.6
7400	5.5	13.7	7853	6.3	7.6
7410	5.7	13.7	7863	6.1	7.5
7420	5.8	13.7	7873	6.0	7.5
7431	6.0	13.6	7883	5.8	7.4
7440	6.2	13.5	7893	5.8	7.4
7450	6.4	13.5	7903	5.6	7.4
7461	6.5	13.4	7909	5.5	7.4
7472	6.6	13.3	7919	5.4	7.4
7480	6.8	13.2	7927	5.3	7.4
7491	7.0	13.1	7932	5.2	7.4
7501	7.1	12.8	7942	5.1	7.4
7510	7.3	12.8	7949	5.0	7.4
7520	7.4	12.6	7958	4.9	7.4
7530	7.5	12.5	7966	4.8	7.4
7541	7.6	12.4	7976	4.7	7.4
7551	7.7	12.2	7987	4.6	7.4
7560	7.8	12.0	7995	4.6	7.4
7571	7.9	11.8	8007	4.4	7.5
7586	8.1	11.6	8017	4.3	7.5
7598	8.1	11.3	8027	4.3	7.5
7606	8.1	11.1	8036	4.2	7.6
7618	8.1	10.8	8045	4.1	7.6
7634	8.1	10.6	8055	4.0	7.6
7643	8.1	10.4	8064	3.9	7.6
7653	8.1	10.3	8073	3.8	7.6
7663	8.1	10.0	8085	3.8	7.7
7674	8.1	9.9	8094	3.7	7.8
7684	8.0	9.7	8106	3.6	7.8
7693	8.0	9.5	8130	3.4	7.9
7703	8.0	9.3	8160	3.2	8.0
7713	7.9	9.2	8200	3.1	8.1
7723	7.9	9.0	8300	2.7	8.6
7734	7.8	8.8	8500	2.2	9.4
7741	7,7	8.6	8700	2.0	9.8
7751	7.6	8.6	8900	1.8	10.3
7762	7.5	8.4	9500	1.6	11.6
7773	7.3	8.2	10000	1.6	12.6

Table 4b
Impedances of the Nickel-200 Ring Near Radial Resonance for the Run in Water: I_{dc} = 3.8 A

Frequency (Hz)	Resistance (Ω)	Reactance (Ω)
9000	7.2	24.1
9040	7.7	24.2
9069	7.9	24.3
9096	8.3	24.4
9122	8.5	24.4
9144	8.8	24.4
9168	9.1	24.4
9187	9.3	24.4
9202	9.6	24.3
9229	9.9	24.2
9261	10.4	24.2
9289	10.9	24.0
9318	11.3	23.8
9351	11.8	23.5
9379	12.2	23.2
9420	12.8	22.7
9465	13.3	22.0
9497	13.6	21.4
9518	13.8	21.0
9558	13.9	20.2
9575	14.0	19.8
9598	14.1	19.4
9621	14.0	18.9
9648	13.9	18.4
9709	13,5	17.2
9741	13.1	16.5
9795	12.4	15.8
9832	11.9	15.4
9892	11.0	14.8
9921	10.5	14.7
9942	10.2	14.6
9961	9.9	14.5
9978	9.7	14.5
9993	9.4	14.5
10025	9.0	14.5
10054	8.6	14.5
10085	8.3	14.6
10114	7.9	14.6
10140	7.6	14.7
10558	4.7	16.6
11037	3.4	19.0

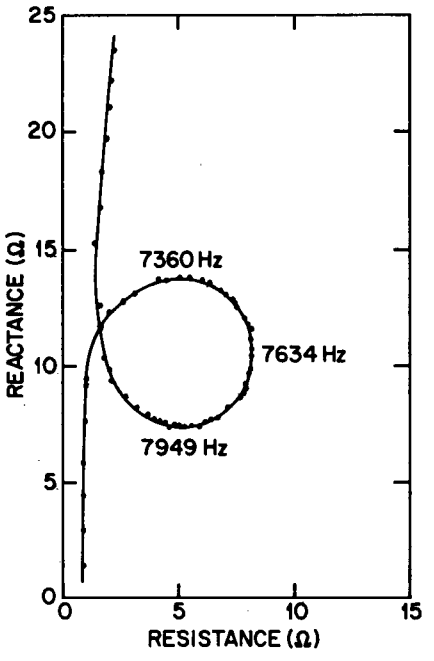

Fig. 5a — Electrical input impedance of the CTN ring in water with I_{dc} = 4.0 A (plotted from Table 4a)

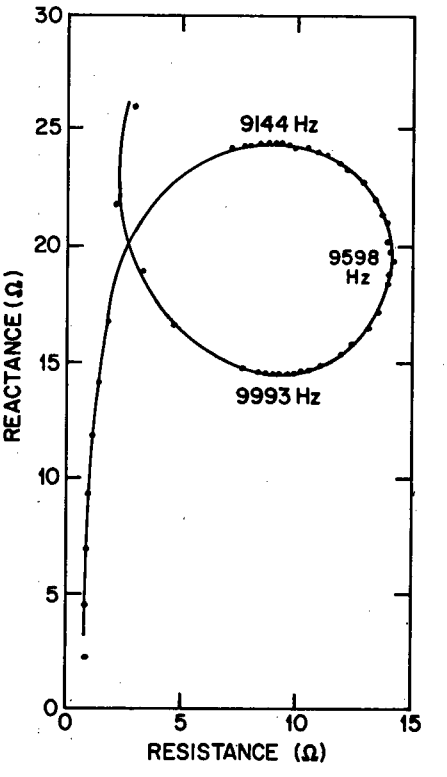

Fig. 5b — Electrical input impedance of the Nickel-200 ring in water with I_{dc} = 3.8 A (plotted from Table 4a)

around the core, μ_{33}^{s} is the reversible permeability at constant strain, χ is the eddy current vector, a is the mean radius of the core (assuming that the thickness of the core is small compared to the diameter), g_{33} is the piezomagnetic constant relating circumferential strain and circumferential magnetic induction in the ring core, S_{33}^{B} is the elastic compliance at constant magnetic induction field of the ring core, R_m is the mechanical resistance, X_m is the mechanical reactance, R_{mp} is the portion of the mechanical resistance due to losses other than eddy-current losses, k_{33} is the material electromechanical coupling coefficient, χ_I is the imaginary part of χ, and M is the mass of the ring core. The symbols chosen for the material constants are consistent with the "IEEE Standard on Magnetostrictive Materials" [2].

The five properties of the CTN ring and the Nickel-200 ring which are derived from the in-air impedance measurements and are then compared are the reversible permeability at constant stress μ_{33}^{T}, the material electromechanical coupling coefficient k_{33}, the elastic compliance S_{33}^{B}, and the effective piezomagnetic strain constants d_{33} and g_{33}. The reversible permeability is obtained from a plot of the low-frequency core reactance versus frequency. At frequencies of excitation of a ring well below the radial resonance frequency the total reactance is given by

$$X_c = \frac{fN^2 4\pi \times 10^{-7}}{a(A_{\text{coil}} - A_0)^{-1}} + \frac{fN^2 \mu_{33}^{T} A_0 \chi_R}{a} ,$$

where χ_R is the real part of χ and is assumed to be unity for the ring cores in this experiment because the thickness of the rings' metal strip is much less than the wavelength of sound in the material over the frequency range of interest. The slope of a plot of X_c versus f is given by

$$\frac{dX_c}{df} = \frac{N^2 4\pi \times 10^{-7}}{a(A_{\text{coil}} - A_0)^{-1}} + \frac{N^2 \mu_{33}^T A_0}{a}$$

$$= \frac{N^2 4\pi \times 10^{-7}}{a} \left[A_{\text{coil}} + \left(\frac{\mu_{33}^T}{4\pi \times 10^{-7}} - 1 \right) A_0 \right].$$

Therefore

$$\mu_{33}^T \approx \frac{a}{A_0 N^2} \frac{dX_c}{df} + 4\pi \times 10^{-7} \left(1 - \frac{A_{\text{coil}}}{A_0} \right). \tag{2}$$

The reversible permeability at constant strain is related to the reversible permeability at constant stress by $\mu_{33}^s = \mu_{33}^T (1 - k_{33}^2)$.

The effective electromechanical coupling coefficient k is calculated from a formula on page 69 in the Summary Technical Report of the National Defense Research Committee [3]:

$$\frac{k^2}{1 - k^2} = \frac{D_Z}{X_c Q_Z}, \tag{3}$$

where D_Z is the diameter of the motional impedance circle in ohms, Q_Z is the quality factor of the transducer, and X_c is the core reactance at the radial resonance frequency. Hysteresis and eddy-current losses are neglected in this formula and in subsequent calculations. The core reactance of a ring at radial resonance is difficult to determine, because it cannot be measured directly. The usual procedure is to measure the core reactance at frequencies well below resonance and well above resonance and extrapolate the resulting curves of core reactance versus frequency to resonance. This method of determining core reactance is complicated by the frequency-dependent hysteresis and eddy-current losses in the ring, which tend to cause the curve to increasingly depart from a straight line at increasing frequencies. For each run in this experiment, curves of core reactance versus frequency were extrapolated to resonance and a value of X_c was estimated. The magnitude of core impedance at resonance was then obtained from the plot of total input electrical reactance versus total input electrical resistance as the magnitude of the impedance vector corresponding to the estimated core reactance. The motional impedance is the total input electrical impedance minus the core impedance. The core impedance was assumed to be constant for the purpose of calculating in-air motional impedances, because the in-air Q values of the rings used in the experiment were large; therefore the range of frequencies corresponding to nonnegligible motional impedances was small. The plot of motional reactance versus motional resistance is a circle called the motional impedance circle. If Z_T, the frequency dependent input impedance, is $R_T + jX_T$, and Z_c, the core impedance, is $R_c + jX_c$, then the motional impedance Z_{mot} is given by

$$Z_{mot} = Z_T - Z_c = R_T - R_c + j(X_T - X_c)$$

and the magnitude of Z_{mot} is given by

$$|Z_{mot}| = [(R_T - R_c)^2 + (X_T - X_c)^2]^{1/2}.$$

The motional impedance was calculated for each run at the frequencies near resonance. The radial resonance frequency f_0 for a run was the frequency corresponding to maximum motional impedance, $|Z_{mot}|_{max}$. The quality factor of a ring transducer is

$$Q_Z = \frac{f_0}{f_2 - f_1},$$

where f_2 and f_1, the quadrantal frequencies, are the frequencies corresponding to $|Z_{mot}| = (1/\sqrt{2})\,|Z_{mot}|_{max}$. The diameter D_Z was measured directly from the plotted motional impedance circle for each run.

The electromechanical coupling coefficient k is the effective coupling coefficient of the ring transducer with leakage inductance present. Though this coupling coefficient is important in transducer applications as an index of performance potential, in material measurements it serves only as an intermediary in the calculation of more basic parameters. The material electromechanical coupling coefficient k_{33} is given [4] by

$$k_{33}^2 = \frac{k^2}{1 - \frac{L_0}{L_f'}\left(1 - \frac{A_0}{A_{coil}}\right)},$$

where L_0 is the inductance of the winding with the ring core removed and L_f' is the free inductance measured at frequencies well below the ring radial resonance frequency:

$$L_0 = \frac{N^2 4\pi \times 10^{-7} A_{coil}}{2\pi a},$$

$$L_f' = \frac{N^2 4\pi \times 10^{-7}}{2\pi a}\,(A_{coil} - A_0) + \frac{N^2 \mu_{33}^T A_0}{2\pi a}.$$

Therefore

$$k_{33}^2 = \frac{k^2}{1 - \frac{\kappa - 1}{\kappa - 1 + \left(\frac{\mu_{33}^T}{4\pi \times 10^{-7}}\right)}}, \tag{4}$$

where $\kappa = \frac{A_{coil}}{A_0}$.

The piezomagnetic strain constants are given by formulas derived from the small-signal linear piezomagnetic transducer equations as indicated in Appendix A:

$$d_{33} = \frac{k_{33}}{\sqrt{1 - k_{33}^2}} \sqrt{\mu_{33}^T S_{33}^B} \ , \tag{5}$$

$$g_{33} = \frac{d_{33}}{\mu_{33}^T} \ . \tag{6}$$

All of the variables on the right sides of Eqs. (5) and (6) are known from previous calculations except S_{33}^B, the elastic compliance. The elastic compliance is calculated from the motional impedance term in Eq. (1). Motional impedance is a maximum when the mechanical reactance X_m goes to zero. This occurs, by definition, at the radial resonance frequency f_0:

$$X_m = 0 = 2\pi f_0 M - \frac{A_0(1 - k_{33}^2)}{a f_0 S_{33}^B} \ ,$$

where

$$S_{33}^B = \frac{(1 - k_{33}^2)A_0}{2\pi M f_0^2 a} \ . \tag{7}$$

The Young's modulus E at constant magnetic induction field is the reciprocal of S_{33}^B.

From an input set of dimensions, electric drive level, selected frequency range, and certain parameters derived from input electrical impedance measurements in air, it is possible, using the NRL computer program NRLEIGSHIP [5], to calculate the total electrical input impedance of a magnetostrictive ring transducer submerged in an unbounded medium and radiating sound. In addition the program delivers in-vacuo modal frequencies, modal shapes, surface velocities, and electrical and mechanical motional impedances. One CTN-ring run (I_{dc} = 4.0 amperes) and one Nickel-200-ring run (I_{dc} = 3.8 amperes) are being used to verify the accuracy of EIGSHIP, and an NRL Report describing the computer program and comparing experimental results to theoretical results will be issued in the near future.

The transmitting efficiency of a transducer in water at resonance is given by an expression also found in the NDRC Report [3]:

$$Eff = \frac{D_w}{R_i} \left[1 - \frac{D_w}{D_Z} \right], \tag{8}$$

where R_i is the total input electrical resistance at water resonance, D_w is the diameter of the motional circle in water, and D_Z is the diameter of the motional circle in air. The transmitting efficiency is the ratio of the acoustic power out to the electrical power in. If all of the electrical power dissipated in the ring were transformed into radiated acoustic power in the far field, the efficiency of the ring would be 100%. However input power

is also dissipated in various loss mechanisms, such as the electrical resistance in the ring windings and the friction, hysteresis and eddy-current losses in the ring core.

CALCULATIONS

The magnetic-field intensities in oersteds shown in Table 2 were calculated from the expression for magnetic field intensity in a toroidally wound coil:

$$H_3 = \frac{NI}{2\pi a} (4\pi \times 10^{-3}),$$

where the mean radius of the coil a is

$$a = \frac{\text{inside diameter + outside diameter}}{4}$$

and $4\pi \times 10^{-3}$ is the conversion factor from MKS units to oersteds. For the CTN ring

$$N = 144 \text{ turns},$$

$$a = 0.06578 \text{ meter},$$

$$H_3 = \frac{144(4\pi \times 10^{-3})}{2\pi(0.06578)} I = 4.38I \text{ 0}e.$$

where I is in amperes. For the Nickel-200 ring

$$N = 144 \text{ turns},$$

$$a = 0.06573 \text{ meters},$$

$$H_3 = \frac{144(4\pi \times 10^{-3})}{2\pi(0.06573)} I = 4.38I \text{ 0}e.$$

The reversible permeability μ_{33}^T was calculated from Eq. (2). For the CTN ring

$$A_0 = 1.349 \times 10^{-4} m^2,$$

$$A_{\text{coil}} = 1.219 \times 10^{-3} m^2,$$

and

$$\mu_{33}^T \text{ (CTN)} = 4\pi \times 10^{-7} \left(1.87 \times 10^4 \frac{dX_c}{df} + 1 - 9.036\right).$$

The plots of low-frequency core reactance X_c versus frequency for the 10 runs on the CTN ring are shown in Fig. 6a. The data points plotted are tabulated in the insert.

For the Nickel-200 ring

$$A_0 = 1.253 \times 10^{-4} m^2,$$

$$A_{\text{coil}} = 1.070 \times 10^{-3} m^2,$$

and

$$\mu_{33}^T \text{ (Nickel 200)} = 4\pi \times 10^{-7} \left(2.01 \times 10^4 \frac{dX_c}{df} + 1 - 8.540 \right).$$

The plots of low-frequency core reactance X_c versus frequency for the 10 runs on the Nickel-200 ring are shown in Fig. 6b.

The slope of each of the lines plotted in Figs. 6a and 6b was measured, the results were inserted in the formulas for μ_{33}^T, and μ_{33}^T was calculated. The 10 values of μ_{33}^T for each ring are plotted against induction field (Fig. 7). The numerical values of μ_{33}^T from which the plots are drawn are given in Table 5. The values of core reactance at ring radial resonance were estimated and are given in Table 6. Also given in Table 6 are the resonance frequencies corresponding to the calculated values of $|Z_{\text{mot}}|_{\text{max}}$, the calculated values of Q_Z, and the measured diameters of the motional impedance circles. The effective electromechanical coupling coefficient k was calculated from Eq. (3) for each run from the values of D_Z, X_c, and Q_Z for each run, and the material electromechanical coupling coefficient k_{33} was calculated from Eq. (4). The coefficient k_{33} is plotted against magnetic induction field in Fig. 8, and the numerical values of k_{33} are given in Table 5. The elastic compliance for each ring was calculated from Eq. (7). For the CTN ring

$$M = 0.4591 \text{ kg},$$

$$S_{33}^B = \frac{(1.349 \times 10^{-4})(1 - k_{33}^2)}{2\pi(0.4591)(0.06578) f_0^2} = 7.109 \times 10^{-4} \frac{(1 - k_{33}^2)}{f_0^2},$$

and

$$E = \frac{1}{S_{33}^B} = 1.407 \times 10^3 \frac{f_0^2}{(1 - k_{33}^2)}.$$

For the 10 runs on the CTN ring the calculated compliance varied between $7.71 \times 10^{-12} m^2/N$ and $8.29 \times 10^{-12} m^2/N$ and the calculated Young's modulus varied between $1.21 \times 10^{11} N/m^2$ and $1.30 \times 10^{11} N/m^2$. For the Nickel-200 ring

$$M = 0.4338 \text{ kg},$$

$$S_{33}^B = \frac{(1.253 \times 10^{-4})(1 - k_{33}^2)}{2\pi(0.4338)(0.06573) f_0^2} = 6.994 \times 10^{-4} \frac{(1 - k_{33}^2)}{f_0^2},$$

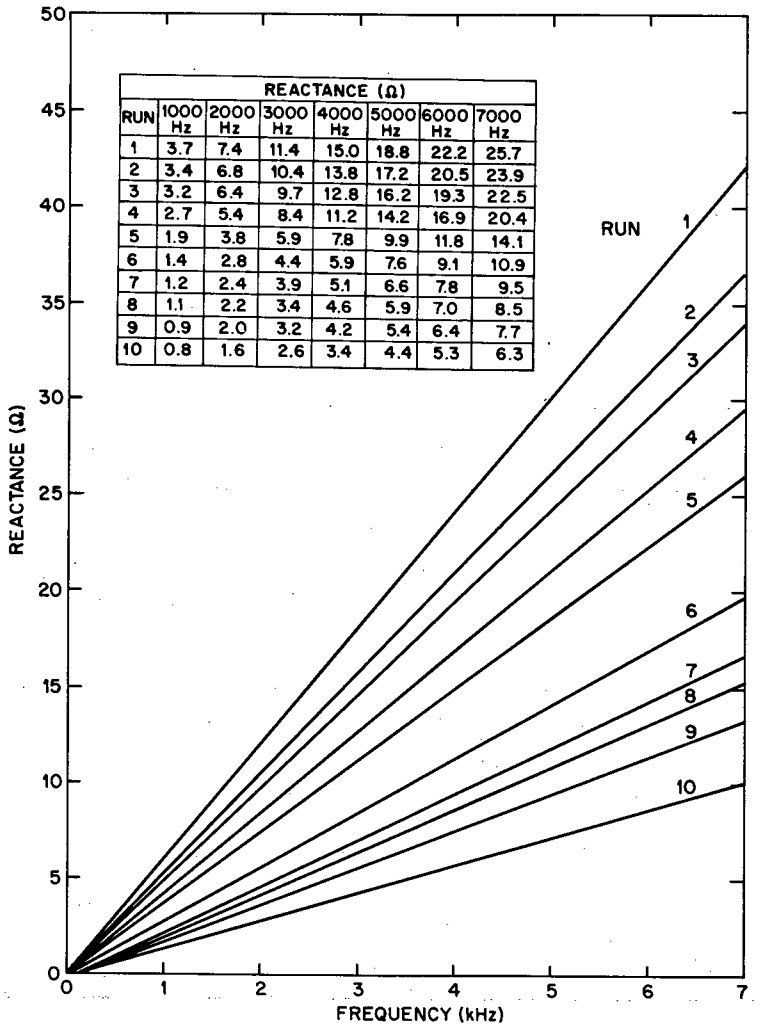

RUN	1000 Hz	2000 Hz	3000 Hz	4000 Hz	5000 Hz	6000 Hz	7000 Hz
1	3.7	7.4	11.4	15.0	18.8	22.2	25.7
2	3.4	6.8	10.4	13.8	17.2	20.5	23.9
3	3.2	6.4	9.7	12.8	16.2	19.3	22.5
4	2.7	5.4	8.4	11.2	14.2	16.9	20.4
5	1.9	3.8	5.9	7.8	9.9	11.8	14.1
6	1.4	2.8	4.4	5.9	7.6	9.1	10.9
7	1.2	2.4	3.9	5.1	6.6	7.8	9.5
8	1.1	2.2	3.4	4.6	5.9	7.0	8.5
9	0.9	2.0	3.2	4.2	5.4	6.4	7.7
10	0.8	1.6	2.6	3.4	4.4	5.3	6.3

Fig. 6a — Low-frequency core reactance of the CTN ring

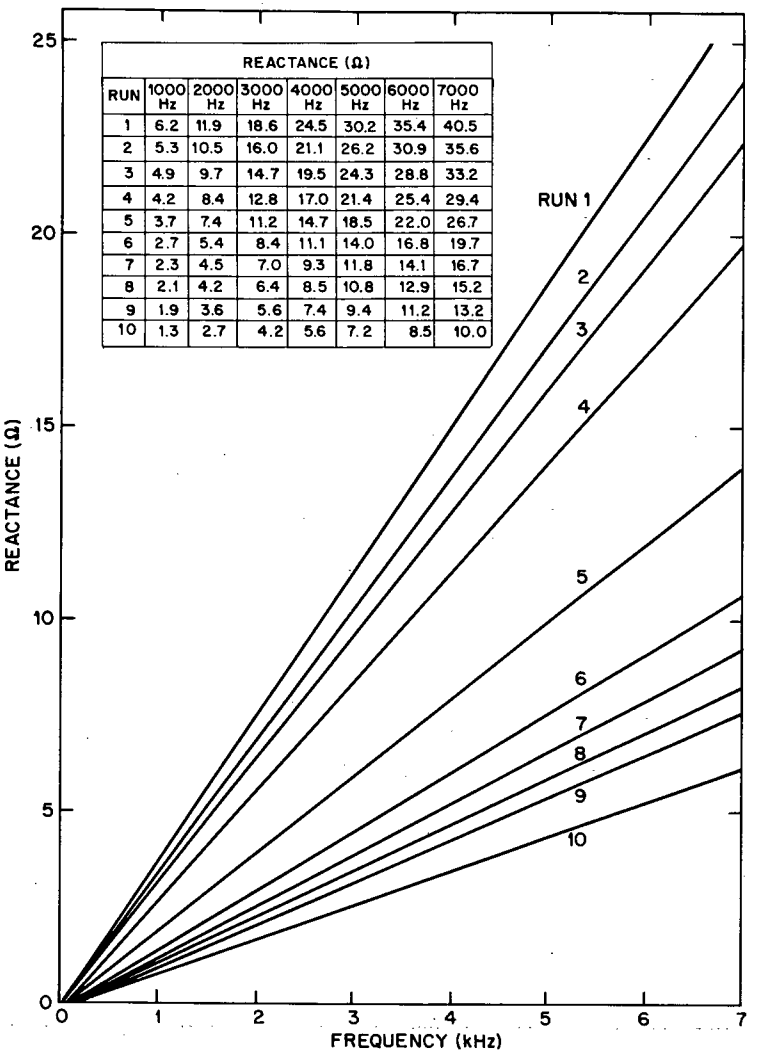

RUN	1000 Hz	2000 Hz	3000 Hz	4000 Hz	5000 Hz	6000 Hz	7000 Hz
1	6.2	11.9	18.6	24.5	30.2	35.4	40.5
2	5.3	10.5	16.0	21.1	26.2	30.9	35.6
3	4.9	9.7	14.7	19.5	24.3	28.8	33.2
4	4.2	8.4	12.8	17.0	21.4	25.4	29.4
5	3.7	7.4	11.2	14.7	18.5	22.0	26.7
6	2.7	5.4	8.4	11.1	14.0	16.8	19.7
7	2.3	4.5	7.0	9.3	11.8	14.1	16.7
8	2.1	4.2	6.4	8.5	10.8	12.9	15.2
9	1.9	3.6	5.6	7.4	9.4	11.2	13.2
10	1.3	2.7	4.2	5.6	7.2	8.5	10.0

Fig. 6b — Low-frequency core reactance of the Nickel-200 ring

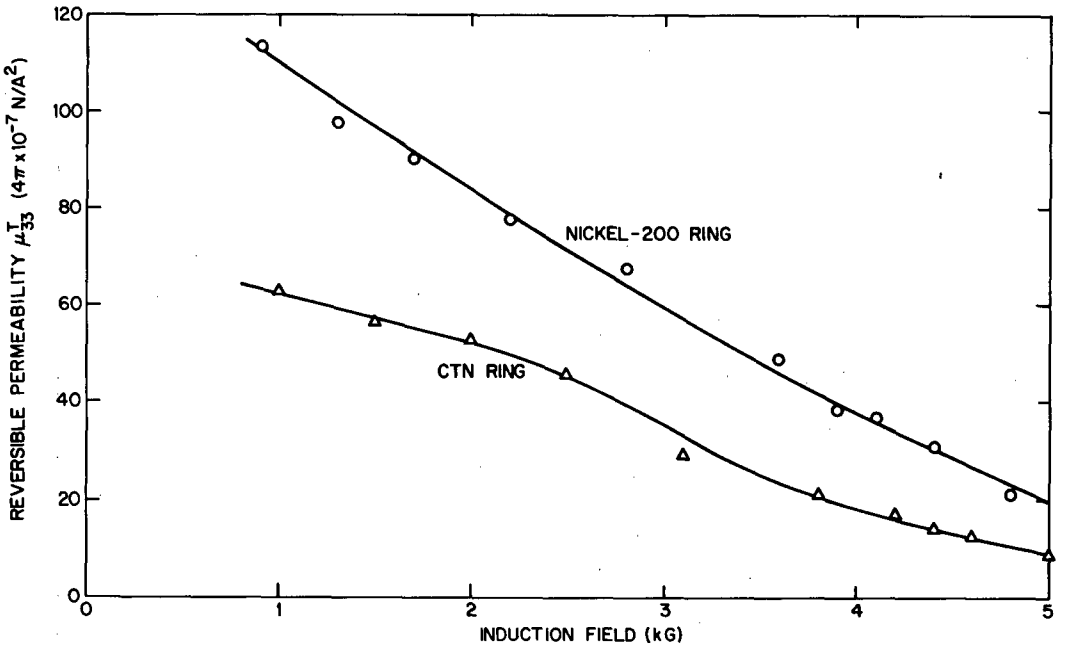

Fig. 7 — Reversible permeability

and

$$E = \frac{1}{S_{33}^B} = 1.430 \times 10^3 \frac{f_0^2}{1 - k_{33}^2}.$$

For the 10 runs on the Nickel-200 ring the calculated compliance varied between $4.88 \times 10^{-12} m^2/N$ and $5.17 \times 10^{-12} m^2/N$ and the calculated Young's modulus varied between $1.93 \times 10^{11}\ N/m^2$ and $2.05 \times 10^{11}\ N/m^2$. The average calculated Young's modulus of the CTN ring is therefore lower than that of the Nickel-200 ring by

$$\frac{1.99 - 1.26}{1.99} \times 100\% = 36.7\%.$$

Since the velocity of sound in the rings is proportional to the square root of the ratio of Young's modulus to density, and the densities of the two rings are roughly the same, then the velocity of sound in the CTN ring is lower than that in the Nickel-200 ring by

$$\frac{\sqrt{1.99} - \sqrt{1.26}}{\sqrt{1.99}} \times 100\% = 20.6\%.$$

The piezomagnetic strain constants were calculated from Eqs. (5) and (6) for each run from the values of S_{33}^B, k_{33}, and μ_{33}^T for each run and are plotted against magnetic induction field in Figs. 9 and 10. The numerical values of d_{33} and g_{33} from which the plots are drawn are given in Table 5.

Table 5
Ring Parameters

Run	Induction Field B_3 (kG)	Reversible Permeability μ_{33}^T ($4\pi \times 10^{-7}\ N/A^2$)	Material Coupling Coefficient k_{33}	Piezomagnetic Constant d_{33} ($10^{-9}\ m/A$)	Piezomagnetic Constant g_{33} ($10^{-5}\ A/N$)
CTN Ring					
1	1.0	62.3	0.067	1.71	2.18
2	1.5	56.3	0.114	2.77	3.92
3	2.0	52.2	0.126	2.95	4.50
4	2.5	45.4	0.162	3.54	6.20
5	3.1	29.4	0.238	4.21	11.4
6	3.8	21.1	0.263	3.94	14.9
7	4.2	17.0	0.280	3.76	17.6
8	4.4	14.0	0.285	3.47	19.7
9	4.6	12.5	0.267	3.07	19.5
10	5.0	8.8	0.281	2.70	24.4
Nickel-200 Ring					
1	0.92	113	0.055	1.49	1.05
2	1.3	97.8	0.110	2.78	2.26
3	1.7	90.1	0.138	3.35	2.96
4	2.2	77.7	0.171	3.87	3.96
5	2.8	67.2	0.219	4.63	5.48
6	3.4	49.1	0.252	4.56	7.39
7	3.9	38.3	0.261	4.17	8.66
8	4.1	36.7	0.261	4.08	8.85
9	4.4	30.7	0.263	3.75	9.72
10	4.8	21.0	0.255	2.99	11.3

Runs 9 and 10 for the CTN ring were done at magnetizing currents of 12 and 20 amperes, resulting in noticeable heating of the ring core (approximately 10°C to 20°C). The effect of increased temperature of the ring core is a decrease in the magnetostriction, which may be visualized as an effective decrease in the induction-field level. Therefore those points on the CTN-ring curves of Figs. 7 through 10 which are plotted at induction

Table 6
Other Ring Parameters Near Air Resonance

Run	Estimated Core Reactance (Ω)	Resonance Frequency (Hz)	Q_Z	Diameter of the Motional Impedance Circle (Ω)
CTN Ring				
1	34.6	9237	185	25.9
2	31.7	9224	132	48.3
3	29.7	9218	130	53.9
4	26.2	9208	110	65.8
5	18.2	9169	98	83.4
6	14.1	9177	107	80.0
7	12.2	9176	112	77.2
8	10.8	9183	121	71.3
9	9.9	9201	161	72.1
10	8.2	9217	174	61.2
Nickel-200 Ring				
1	58.	11608	153	25
2	54.	11595	105	64
3	49.	11579	90	80
4	44.5	11556	77	94
5	39.	11499	65	115
6	32.	11471	64	120
7	26.2	11485	72	114
8	25.1	11491	78	118
9	21.7	11511	91	116
10	16.4	11581	127	105

field levels 4.6 and 5.0 kilogauss actually correspond to lower effective induction-field levels, but the temperature correction is not known.

The experimental results near air resonance for the CTN ring at I_{dc} = 4.0 amperes presented in Table 3a were used to calculate the in-air motional impedance, resonance frequency, and quality factor as an example of these calculations for a CTN-ring run.

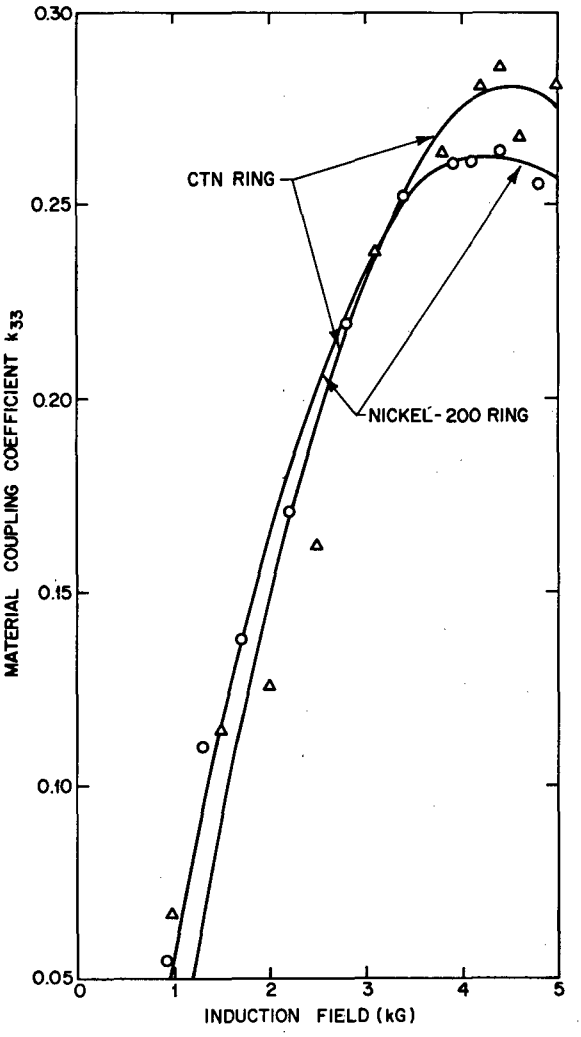

Fig. 8 — Effective coupling coefficient

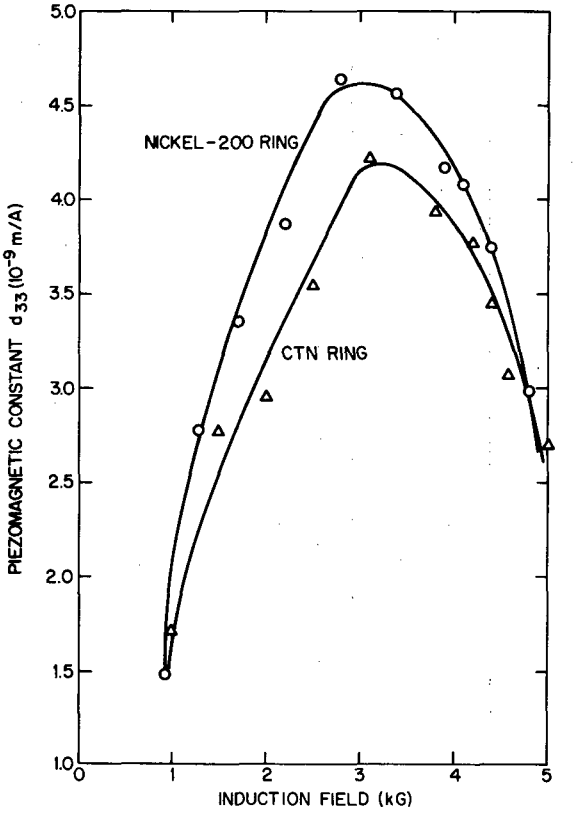

Fig. 9 — Piezomagnetic constant d_{33}

The core reactance and resistance at in-air resonance, which were extrapolated from the curves of core reactance off resonance and the plot of total reactance versus resistance, were estimated to be 14.1 ohms and 0.6 ohm. These values were subtracted from the total input reactance and resistance values of Table 3a, and the resulting motional reactance is plotted against motional resistance in Fig. 11a. The values of motional impedance are given in Table 7a. The frequency corresponding to maximum motional impedance is 9177 Hz, and the diameter of the circle drawn from the origin to the point of $|Z_{mot}|_{max}$ shows that the circle is inclined from the horizontal by an angle of 8 degrees. The circle tilt is a measure of hysteresis and eddy-current losses. The quadrantal frequencies f_1 and f_2 corresponding to $|Z_{mot}| = (1/\sqrt{2})\,|Z_{mot}|_{max}$ are 9140 Hz and 9226 Hz. The quality factor in air is

$$Q_Z = \frac{9177}{9226 - 9140} = \frac{9177}{86} = 107.$$

The diameter of the motional impedance circle is 80 ohms.

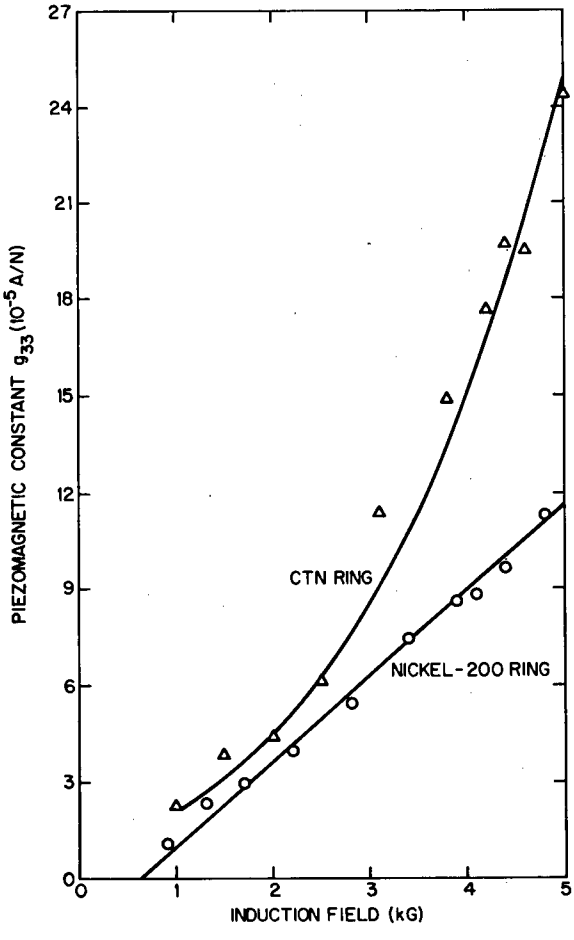

Fig. 10 — Piezomagnetic constant g_{33}

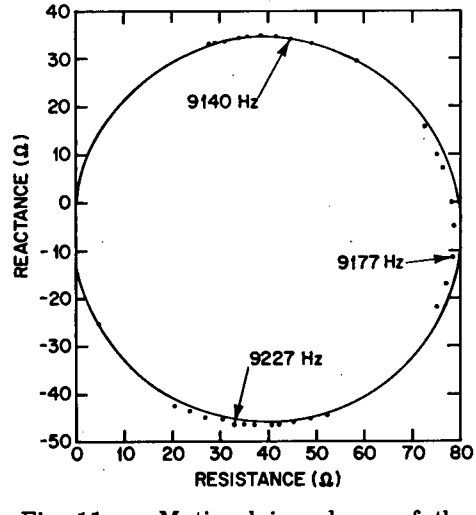

Fig. 11a — Motional impedance of the CTN ring in air with I_{dc} = 4.0 A

Table 7a
Motional Impedance of the CTN Ring
in Air When I_{dc} = 4.0 A

Frequency (Hz)	Resistance (Ω)	Reactance (Ω)
8000	—	—
8500	—	—
9000	—	—
9119	27.9	32.7
9122	29.2	33.2
9125	30.8	33.6
9128	33.7	34.1
9131	35.8	34.3
9134	38.4	34.4
9137	41.4	34.3
9140	44.4	34.0
9144	49.1	33.0
9150	58.2	29.4
9162	72.4	15.6
9165	75.2	10.0
9168	76.3	7.2
9171	78.1	0
9174	78.6	-5.1
9177	78.3	-11.8
9180	77.2	-16.8
9184	75.4	-22.0
9206	52.1	-44.3
9209	48.6	-45.3
9212	45.4	-46.0
9215	42.0	-46.5
9218	40.4	-46.6
9221	36.9	-46.6
9224	34.7	-46.5
9227	32.7	-46.3
9230	30.2	-45.8
9233	27.2	-45.0
9239	23.6	-43.8
9246	20.3	-42.2
9321	4.5	-25.5
9500	—	—
10000	—	—
11000	—	—

The experimental results near air resonance for the Nickel-200 ring at I_{dc} = 3.8 amperes presented in Table 3b were used to calculate the in-air motional impedance, resonance frequency, and figure of merit as an example of these calculations for a Nickel-200-ring run. The core reactance and resistance at in-air resonance were estimated to be

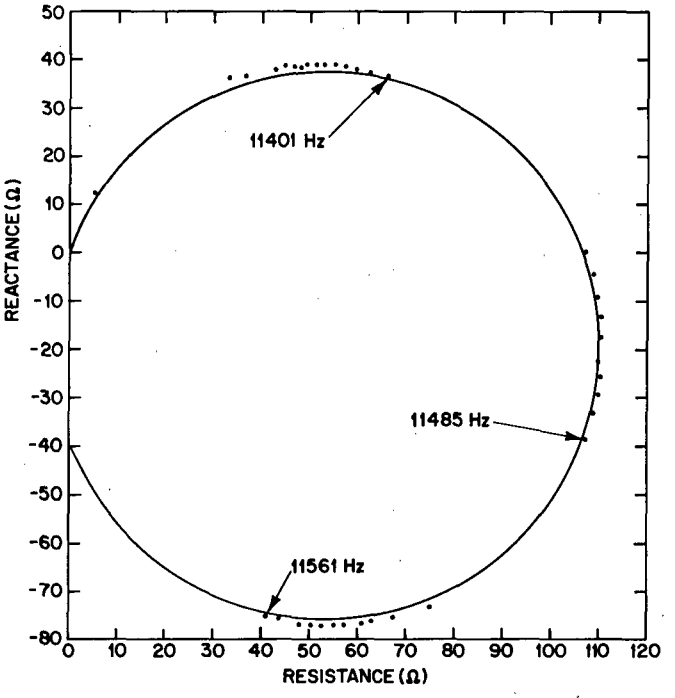

Fig. 11b — Motional impedance of the Nickel-200 ring in air with I_{dc} = 3.8 A

26.2 ohms and 3.6 ohms. These values were subtracted from the total input reactance and resistance values of Table 3b, and the resulting motional reactance is plotted against motional resistance in Fig. 11b. The corresponding values of motional impedance are given in Table 7b. The frequency corresponding to maximum motional impedance is 11485 Hz, and the circle is inclined from the horizontal by an angle of 19 degrees. The quadrantal frequencies f_1 and f_2 corresponding to $|Z_{mot}| = (1/\sqrt{2})\ |Z_{mot}|_{max}$ are estimated to be 11,410 Hz and 11,569 Hz. Impedance measurements were not taken at these frequencies, but they were extrapolated from the closest measured impedance values. The quality factor in air is

$$Q_Z = \frac{11485}{11569 - 11410} = 72.$$

The diameter of the motional impedance circle is 114 ohms.

Each of the other runs for both rings were analyzed in accordance with the methods indicated in these examples.

The motional impedance circles in water are not plotted, because their tilts are a sensitive function of the estimated core reactances at water resonance frequency. For example a 1-ohm error in the estimate of the core reactance for the CTN ring (I_{dc} = 4.0 amperes) at the water resonance frequency will change the tilt of the water motional-impedance circle by 7 degrees. The Pulse Vector Immittance Meter had a system error of ±1 ohm and a reading error of ±0.1 ohm. The system error was manifest in the error in the measured reactance of a standard inductor. Consequently all of the electrical

Table 7b
Motional Impedance of the Nickel-200 Ring
in Air When I_{dc} = 3.8 A

Frequency (Hz)	Resistance (Ω)	Reactance (Ω)
8000	—	—
9000	—	—
10000	—	—
11000	5.1	12.2
11333	32.7	36.2
11345	36.4	37.0
11360	42.6	38.0
11364	44.5	38.5
11368	46.7	38.4
11371	47.9	38.6
11374	48.9	39.6
11377	50.9	39.3
11381	52.8	39.2
11384	55.1	39.0
11388	57.1	38.5
11392	59.6	38.0
11396	62.1	37.5
11401	66.0	36.5
11455	107.3	0.3
11459	109.0	-4.4
11462	109.5	-9.3
11466	110.6	-13.4
11469	111.0	-17.5
11472	110.4	-22.3
11475	110.4	-25.8
11478	109.6	-29.1
11481	108.8	-33.0
11485	107.6	-38.2
11525	74.9	-73.2
11532	67.5	-75.4
11535	63.1	-76.2
11538	60.7	-76.6
11541	57.4	-76.8
11544	55.0	-77.0
11547	52.2	-77.0
11550	50.1	-76.8
11554	47.9	-76.6
11558	43.6	-75.9
11561	41.2	-75.3

resistance and reactance readings may be too great or too small by as much as 1 ohm. The reading error was manifest in an uncertainty in the last digit of all of the measured impedance values.

The transmitting efficiencies *Eff* of the rings in water at their separate resonances were calculated from Eq. (8). Though the tilts of the motional impedance circles in water are a sensitive function of the estimated core reactances at water resonance frequency, the diameters of the motional impedance circles are relatively insensitive to the choice of core reactances. The in-water impedance curves shown in Figs. 5a and 5b are plots of total electrical reactance against total electrical resistance. To find the corresponding motional-impedance curves, the core impedance was subtracted from the total impedance at each frequency represented by a data point. Because the Q of the rings was low in water (approximately 10 to 15), a different value of core impedance was used for each data point. The rate of change of core reactance with frequency was extrapolated from the low-frequency-core-impedance plots of Figs. 6a and 6b.

For the CTN ring at $I_{dc} = 4.0$ amperes

$$D_Z = 80.0 \text{ ohms},$$

$$R_i = 8.1 \text{ ohms},$$

$$D_w = 7.2 \text{ ohms},$$

$$E_{ff} = \frac{7.2}{8.1}\,\frac{80 - 7.2}{80} = 0.81 \Rightarrow 81\%,$$

For the Nickel-200 ring at $I_{dc} = 3.8$ amperes

$$D_Z = 114 \text{ ohms},$$

$$R_i = 14.1 \text{ ohms},$$

$$D_w = 11.9 \text{ ohms},$$

$$E_{ff} = \frac{11.9}{14.1}\,\frac{114 - 11.9}{114} = 0.76 \Rightarrow 76\%.$$

The transmitting efficiencies of the rings were also calculated from the ratio of the acoustic power out to the electrical power in for each ring. The acoustic power out was found by numerically integrating under the far-field directivity patterns corresponding to the rings' in-water resonance frequencies. For detectable far-field transmission however the rings were driven at currents of 100 milliamperes ac. The efficiencies determined by this method were 59% for the CTN ring and 66% for the Nickel-200 ring. These numbers differ from the previously calculated efficiencies because of uncertainties and approximations used in both calculations. The efficiencies are high because the ac driving currents were small. The purpose of doing the calculations was to indicate that at low-power drive the efficiences of the two rings were comparable.

Interesting speculation can be made relevant to the use of the rings in a *billboard* array. A *billboard* array is a row of coaxial stacks of elements. The number, spacing, and

amplitude shading of the elements in a stack determine the acoustic radiation profile in the vertical planes (planes parallel to the axes of the stacks). The number, spacing, and amplitude shading of the stacks in the row determine the acoustic radiation profile in the horizontal planes (planes perpendicular to the axes of the stacks). Since the CTN ring used in this experiment had a 20% lower resonance frequency than the Nickel-200 ring of the same dimensions, and since ring resonance frequency is inversely proportional to ring diameter, a CTN ring with the same resonance frequency as the Nickel-200 ring would have a 20% smaller diameter. Therefore a CTN-ring array could be more densely packed than a Nickel-200-ring array operated at the same resonance frequency, resulting in a reduction of the interelement spacing and a greater angular displacement of all of the minor lobes from the main beam of the CTN array radiation pattern. On the other hand, if a CTN-ring array were built with the same interelement spacing used in a Nickel-200 ring array and the resonance frequencies of the rings in each array were identical, then the smaller CTN rings would be acoustically less visible and have less mutual coupling between elements than the larger Nickel-200 rings.

CONCLUSIONS

The comparison between the CTN and the Nickel-200 magnetostrictive free-flooded ring transducers shows the relative advantages and disadvantages of each ring. Because the ac excitation current for all of the runs was only 15 milliamperes, the comparison is based on measurements which were made at low-power and linear excitation.

Figure 7 shows that at any specified induction-field level over the induction-field range 1 to 5 kilogauss the reversible permeability μ_{33}^T of the CTN ring is approximately 1/2 that of the Nickel-200 ring. The input core electrical impedance, which is proportional to the reversible permeability, of the CTN ring is correspondingly less than that of the Nickel-200 ring when both rings are excited at the same frequency. The eddy-current loss in a magnetostrictive ring is also proportional to the reversible permeability, whose smaller value for the CTN ring is an advantage manifest in reduced internal heating losses. The higher permeability of the Nickel-200 ring does however have an important advantage that is revealed in Table 2. The Nickel-200 ring requires a smaller ampere-turn product than the CTN ring to achieve a specified level of magnetic induction field.

The material electromechanical coupling coefficients of the two rings strongly depend on induction field level, with the CTN ring achieving a slightly higher value of coupling coefficient ($\approx$7%) at optimum levels of magnetizing induction field ($\approx$4 kilogauss). The piezomagnetic strain constant d_{33} is slightly higher ($\approx$8%) at optimum magnetization for the Nickel-200 ring. The significance of d_{33} in terms of the piezomagnetic activity of a material is in its relationship to k_{33}, a relationship which involves the other material parameters S_{33}^H and μ_{33}^T. A measure of the energy conversion capability of the ring is given by k_{33}^2, because it "gives the fraction of input electrical energy which appears in mechanical form, stored in the elastic displacement" [6]. The curves of g_{33} versus B_3 in Fig. 10 show a much greater slope for the CTN ring than for the Nickel-200 ring. Since g_{33} relates strain to magnetic induction field in the transducer, the greater slope of the CTN ring curve tends to confirm the claim that CTN has a higher "available magnetostrictive strain energy" [7].

A clearly desirable advantage of the CTN ring over the Nickel-200 ring is the 37% lower Young's modulus, resulting in a 21% lower sound velocity. In practical terms this means that to satisfy a specified resonance frequency requirement, a CTN ring can be built with a 21% smaller diameter than a Nickel-200 ring, resulting in correspondingly lighter weight, easier handling, and lower fabrication costs.

The quality factor Q_Z (Table 6) of the CTN ring is greater than that of the Nickel-200 ring at any specified field level over the induction field range because of the smaller internal heating losses resulting from the smaller reversible permeability of the CTN ring. Consequently the ratio of the diameter of the Nickel-200 motional impedance circle at I_{dc} = 3.8 amperes (3.9-kilogauss induction field) to the diameter of the CTN motional impedance circle at I_{dc} = 4.0 amperes (3.8-kilogauss induction field) is only 1.4, whereas the ratio of the corresponding $[\mu_{33}^T g_{33}/S_{33}^B]^2$ terms in Eq. (1) is 3.7. This result implies that most of the surface-velocity disadvantage of the CTN ring due to its lower permeability is made up by its larger Q_Z and lower resonance frequency in comparison to the Nickel-200 ring. The impedance circles in water shown in Fig. 5, which were taken at the same values of magnetizing currents (and induction fields) used in air, support the conclusions based on the impedance circles in air. The water resonance frequency of the CTN ring is approximately 20% lower than the water resonance frequency of the Nickel-200 ring. A smaller ring for the same resonance frequency results in an advantage for the CTN ring as an element of an array of rings. Finally the transmitting efficiency of the CTN ring is approximately the same as that of the Nickel-200 ring when they are compared at their different water resonance frequencies.

The power-handling capability, which is an important property of magnetostrictive ring transducers, can be determined only by experiments at high power drive.

Other comparisons are possible between the two rings based on the data presented in this report or using the computer model of a magnetostrictive ring. The purpose of this experiment however was to provide enough information to familiarize the transducer engineer with the properties of a CTN ring and to allow him to choose which type of magnetostrictive ring will best fit a low-power linear-drive application.

ACKNOWLEDGMENTS

The author is grateful to E. L. Huston of the International Nickel Co., Suffern, New York, for preparing the CTN ring and for his many valuable suggestions about the presentation of the data. Gratitude is also expressed to C. LeBlanc of the Underwater Systems Center, New London, Connecticut, for a valuable tutorial communication on piezomagnetic material constants. Valuable discussions were held with J. Trott, R. Woollett, R. Baier, and R. Rojas. J. Neeley took most of the impedance measurements.

REFERENCES

1. S. Butterworth and F.D. Smith, "The Equivalent Circuit of the Magnetostriction Oscillator," *Phys. Soc.* 43 (No. 2), 166 (1931).

2. "IEEE Standard on Magnetostrictive Materials: Piezomagnetic Nomenclature," Technical Committee on Transducers and Resonators of the IEEE Group on Sonics and Ultrasonics, The Institute of Electrical and Electronics Engineers, 1971.

3. "The Design and Construction of Magnetostriction Transducers," Volume 13 of the Summary Technical Report of Division 6, National Defense Research Committee, Washington, D.C., 1946.

4. R.S. Woollett, "Electromechanical Evaluation of Magnetostrictive Cylinders by Resonance-Antiresonance Measurements," USN Underwater Sound Laboratory Research Report 225, 15 Dec. 1953.

5. S. Hanish, R.V. Baier, B.J. King, P.H. Rogers, and J.A. Sinsky, "A Mathematical Model of the Electroacoustic Performance of a Free-Flooded Magnetostrictive Shell," to be submitted for publication to the Journal of the Acoustical Society of America.

6. R.S. Woollett, "Magnetostrictive Material Requirements for Sonar Transducers," *U.S. Navy Journal of Underwater Acoustics* 20 (No. 4), 679 (1970).

7. E.L. Huston, D.T. Peters and G.D. Sandrock, "Magnetic and Magnetostrictive Properties of Cube Textured Nickel for Magnetostrictive Transducer Applications." *IEEE Transactions on Magnetics* MAG-9 (No. 4), 636 (Dec. 1973).

Appendix A
THE DERIVATIONS OF THE EQUATIONS FOR d_{33} AND g_{33}

The author is indebted to Mr. Charles LeBlanc Underwater Systems Center, New London, Connecticut, for a private communication which derived and showed the importance of using the appropriate piezomagnetic constants.

For thin rings* (in MKS units)

$$S_3 = S_{33}^H T_3 + d_{33} H_3 \tag{A1}$$

and

$$B_3 = d_{33} T_3 + \mu_{33}^T H_3, \tag{A2}$$

where

S_3 = the circumferential strain,

T_3 = the circumferential stress,

B_3 = the circumferential magnetic induction field,

H_3 = the circumferential magnetic field intensity,

S_{33}^H = the elastic compliance at constant H,

d_{33} = the piezomagnetic constant,

μ_{33}^T = the reversible permeability at constant T.

The material electromechanical coefficient k_{33} is given by

$$k_{33}^2 = \frac{d_{33}^2}{S_{33}^H \mu_{33}^T},$$

where

$$S_{33}^B = S_{33}^H (1 - k_{33}^2).$$

*R.S. Woollett, "Magnetostrictive Material Requirements for Sonar Transducers," U.S. Navy Journal of Underwater Acoustics 20 (No. 4), 679 (1970).

Therefore

$$k_{33}^2 = \frac{d_{33}^2(1 - k_{33}^2)}{S_{33}^B \mu_{33}^T}$$

and

$$d_{33} = \frac{k_{33}}{\sqrt{1 - k_{33}^2}} \sqrt{\mu_{33}^T S_{33}^B}.$$

The piezomagnetic constant g_{33} is defined by the equation*

$$S_3 = S_{33}^B T_3 + g_{33} B_3.$$

Substituting for B_3 from Eq. (A2),

$$\begin{aligned} S_3 &= S_{33}^B T_3 + g_{33}[d_{33} T_3 + \mu_{33}^T H_3] \\ &= [S_{33}^B + g_{33} d_{33}] T_3 + g_{33} \mu_{33}^T H_3. \end{aligned}$$

Comparing the coefficient of H_3 with the corresponding coefficient in Eq. (B1),

$$g_{33} \mu_{33}^T = d_{33}$$

or

$$g_{33} = \frac{d_{33}}{\mu_{33}^T}.$$

*Technical Committee on Transducers and Resonators of the IEEE Group on Sonics and Ultrasonics, "IEEE Standard on Magnetostrictive Materials: Piezoelectric Nomenclature," The Institute of Electrical and Electronics Engineers, 1971.